Control of solvated crystallization of α-lactose (alpha-lactose) monohydrate

Amira Rachah, Dominikus Noll, Fabienne Espitalier, Fabien Baillon

Control of solvated crystallization of α-lactose monohydrate

A. Rachah * D. Noll * F. Espitalier † F. Baillon †

Abstract

We present a mathematical model of solvated crystallization of α-lactose monohydrate and discuss strategies to control the crystallization process in semi-batch mode with the goal to privilege the production of small particles in the range between $130\,\mu m$ and $330\,\mu m$. We compare specific and unspecific cost functions leading to optimal strategies with significantly different effects on product quality. Control inputs are temperature, feed rate, and the choice of an appropriate crystal seed.

Keywords: Solvated crystallization, population dynamics, molar balance, thermodynamic balance, optimal control.

1 Introduction

Crystallization is the unitary operation of formation of solid crystals from a liquid solution. In process engineering crystallization is an important separation technique used in chemical, pharmaceutical, food, material and semiconductor industries. Mathematical models of crystallization processes include population, molar and energy balance equations. Crystallizers can be operated in batch, semi-batch or continuous mode.

Semi-batch crystallization is widely used in the pharmaceutical and fine chemical industry for the production of solids in a variety of operating modes. In the food-processing industry, there has been growing interest in the crystallization of lactose in recent years [17, 18, 20]. For a number of reasons, α-lactose monohydrate is the most commonly used form of lactose in making medications. It is for instance affordable, physically and chemically stable, easy to mix, readily dissolves in but does not absorb water.

Lactose monohydrate is available as a powder in different grades, density, and flowability. Here we present a mathematical model of solvated crystallization of α-lactose monohydrate, and then use it to control the crystallization process in semi-batch mode in such a way that the growth of crystals in the range $130\,\mu m$ to $330\,\mu m$ is privileged to enhance flowability.

The model shown schematically in Figure 1 combines the dynamics of four interacting populations, one of them aging, governed by an energy balance. For a schematic view of the crystallizer see Figure 8.

*Université Paul Sabatier, Institut de Mathématiques, Toulouse, France
†Ecole des Mines d'Albi, Laboratoire Rapsodee, Albi, France

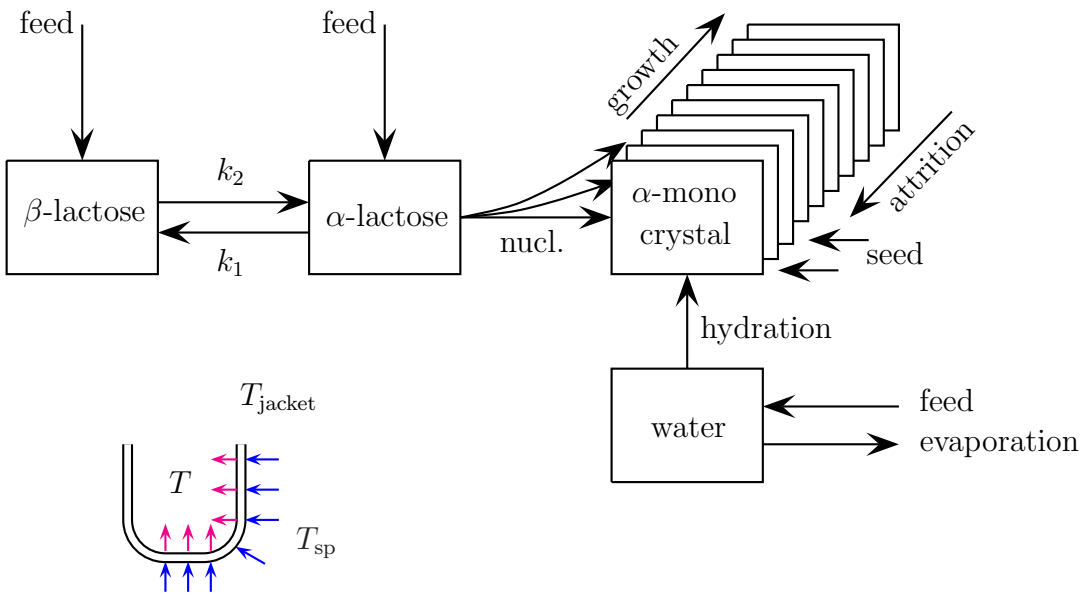

FIGURE 1: Crystallization of α-lactose monohydrate

Two forms of lactose (α- and β-lactose) exist simultaneously in aqueous solution, the exchange being described by the process of mutarotation with exchange rates k_1, k_2. For temperatures $T \leq 90\,^{\circ}C$ only α-lactose crystallizes, with the specificity that a water molecule is integrated at the formation of an α-crystal. Nucleation and growth of crystals are the basic mechanisms, which may be complemented by modeling attrition, breakage, agglomeration and secondary nucleation effects. Here we are interested in semi-batch crystallization, where the container is initially only partially filled. By acting on the feed rate, the temperature, and on the crystal seed, we wish to steer the process in such a way that the growth of particles within the size range $130\,\mu m \leq L \leq 330\,\mu m$ is maximized.

Active and passive control strategies for crystallization processes have been used in batch, semi-batch, or continuous mode to improve product quality, to maximize the final size of crystals, to guarantee process stability, and much else. We mention approaches of a general nature in off-line optimal control of crystallization processes in [5, 10, 11]. Concerning modeling and control of α-lactose monohydrate, there is a large body of experimental work using heuristic control strategies [16–18, 20, 21]. In [30] optimization methods have been applied to a PDE model of crystallization of the inorganic compound, potassium aluminum sulfate $KAl(SO_4)_2$ in water, but the present work is not covered by this approach. Our approach to control the crystallization of α-lactose monohydrate by means of a mathematical model using balance equations is new. Our results based on optimal control strategies will therefore be compared to heuristic methods known in the literature.

The structure of the paper is as follows. In section 2 we develop the model. In Section 3 a model for control based on a moment approximation is obtained, which is then used in section 4 to compute numerical results.

2 Dynamic model

In this section the dynamic model of semi-batch crystallization of α-lactose monohydrate is described by presenting the population, mass and energy balance equations.

2.1 Population balance equation

The population balance equation is a first-order PDE

$$\frac{\partial}{\partial t}\left(V(t)n(L,t)\right) + V(t)G\left(c_\alpha(t), c_\beta(t), T(t)\right)\frac{\partial n(L,t)}{\partial L} = V(t)\dot{n}(L,t)^{\pm}, \tag{1}$$

where $n(L,t)$ is the distribution of α-lactose crystals (CSD), that is, the number of α-lactose crystals per unit volume $1\,m^3$ and per unit length $1\,m$, expressed as $number \cdot m^{-3} \cdot m^{-1}$. The quantities $c_\alpha(t), c_\beta(t)$ are the dimensionless concentrations of α- and β-lactose in the liquid phase, that is

$$m_\alpha = c_\alpha m_{\mathrm{H_2O}}, \quad m_\beta = c_\beta m_{\mathrm{H_2O}},$$

where m_α, m_β represent respectively the mass of α- and β-lactose in the liquid phase, $m_{\mathrm{H_2O}}$ the mass of water not integrated in crystals.

The total volume of slurry $V(t)$ in the crystallizer is a dependent variable given in (15), $G\left(c_\alpha, c_\beta, T\right)$ is the temperature-dependent growth coefficient of α-crystals, or put differently, the *velocity* of crystal growth in $m \cdot s^{-1}$, assumed independent of crystal size L. We add the boundary condition

$$n(0,t) = \frac{B\left(c_\alpha(t), c_\beta(t), T(t)\right)}{G\left(c_\alpha(t), c_\beta(t), T(t)\right)}, \tag{2}$$

which involves the temperature dependent birth coefficient $B(c_\alpha, c_\beta, T)$, the velocity of nucleation or crystal birth in $number \cdot m^{-3} \cdot s^{-1}$. Finally, the initial condition

$$n(L,0) = n_0(L), \tag{3}$$

represents the *crystal seed* $n_0(L)$. Crystal size L is measured in meters m, time t in seconds s.

The right hand side of (1) features source and sink terms $\dot{n}(L,t)^{\pm} = \dot{n}(L,t)^{+} - \dot{n}(L,t)^{-}$, which may include breakage, attrition and agglomeration of crystals, and possibly removal of crystals due to outflow, filtering, or fines dissolution. In the case of attrition or breakage the source terms are

$$\dot{n}^{+}(L,t) = \int_{2^{1/3}L}^{\infty} b(L')\beta(L' \to L)n(L',t)dL' + \int_{L}^{2^{1/3}L} b(L')\beta(L' \to L'')n(L',t)dL', \tag{4}$$

where $L'' = (L'^3 - L^3)^{1/3}$, and

$$\dot{n}^{-}(L,t) = b(L)n(L,t).$$

Here $b(L)$ is the breakage rate of particles of size L, with unit s^{-1}, and $\beta(L' \to L)$ is the daughter size distribution with unit m^{-1}. We assume breakage of a crystal of size L' into two daughters of sizes L and L'', where $L^3 + L''^3 = L'^3$. In order to break the symmetry, we assume that $\beta(L' \to L)$ is only defined for $L \in [2^{-1/3}L', L']$, that is for $L \geq L'' = (L'^3 - L^3)^{1/3}$. Moreover, $\int_{2^{-1/3}L'}^{L'} \beta(L' \to L)dL = 1$. This explains the two integral terms in (4). The left hand term counts those events, where a particle of size L' breaks into pieces L, L'' with $L \geq L'$, so we have a new particle of size L arriving. The second term counts those events, where L' breaks into pieces L'', L with $L'' \geq L$. Now the smaller piece contributes to the source at size L.

quantity	symbol	unit
breakage rate	$b(L)$	s^{-1}
daughter size distribution	$\beta(L' \to L)$	m^{-1}
agglomeration rate	$\alpha(L' \to L)$	$m^3 \sharp^{-1} s^{-1}$
crystal seed	$n_0(L)$	$\sharp/m.m^3$

TABLE 1: Size related quantities

2.2 Relating crystal mass to CSD

We consider the mass $m_{\text{cry}}(t)$ of mono-hydrated α-lactose crystals as a function of time and relate it to the crystal size distribution $n(L,t)$ through

$$m_{\text{cry}}(t) = k_v \rho_{\text{cry}} V(t) \int_0^\infty n(L,t) L^3 dL.$$

Introducing the third moment

$$\mu_3(t) = \int_0^\infty n(L,t) L^3 dL$$

of the CSD, this may be written as

$$m_{\text{cry}}(t) = k_v \rho_{\text{cry}} V(t) \mu_3(t).$$

Therefore, by applying the product rule, substituting (1), and using partial integration, we have

$$\begin{aligned} \frac{dm_{\text{cry}}(t)}{dt} &= k_v \rho_{\text{cry}} \frac{dV(t)}{dt} \int_0^\infty n(L,t) L^3 dL + k_v \rho_{\text{cry}} V(t) \int_0^\infty \frac{\partial n(L,t)}{dt} L^3 dL \\ &= -k_v \rho_{\text{cry}} G(c_\alpha(t), c_\beta(t), T(t)) V(t) \int_0^\infty \frac{\partial n(L,t)}{dL} L^3 dL \\ &= 3 k_v \rho_{\text{cry}} G(c_\alpha(t), c_\beta(t), T(t)) V(t) \int_0^\infty n(L,t) L^2 dL \qquad (5) \\ &= 3 k_v \rho_{\text{cry}} G(c_\alpha(t), c_\beta(t), T(t)) V(t) \mu_2(t), \end{aligned}$$

where μ_2 is the second moment of the CSD,

$$\mu_2(t) = \int_0^\infty n(L,t) L^2 dL.$$

Here we use the hypothesis that all external birth and death processes of crystals are mass preserving, i.e., that

$$\int_0^\infty \left(\dot{n}(L,t)^+ - \dot{n}(L,t)^- \right) L^3 dL = 0. \qquad (6)$$

That includes breakage, attrition, agglomeration of monohydrated α-lactose crystals, but excludes product removal or seeding during the process.

The initial condition associated with (5) is

$$m_{\mathrm{cry},0} = k_v \rho_{\mathrm{cry}} V_0 \int_0^\infty n_0(L) L^3 dL = k_v \rho_{\mathrm{cry}} V_0 \mu_{3,0},$$

which fixes the third moment of the crystal seed $n_0(L)$ to

$$\mu_{3,0} = \frac{m_{\mathrm{cry},0}}{k_v \rho_{\mathrm{cry}} V_0}. \tag{7}$$

2.3 Solvent mass balance

The particularity of solvated crystallization is that the variations of solvent mass, $\frac{dm_{\mathrm{H_20}}}{dt}$, and of crystal mass, $\frac{dm_{\mathrm{cry}}}{dt}$, are coupled. The fact that α-lactose crystals integrate a water molecule means that molecular weights of the solid and liquid phase of α-lactose are related as

$$R = \frac{M_{\mathrm{cry}}}{M_\alpha} = 1.0525 > 1. \tag{8}$$

Therefore, if we temporarily define the mass of water inside crystals as $m_{\mathrm{H_20 \subset cry}}$, we have

$$m_{\mathrm{H_20 \subset cry}} = \left(1 - \frac{1}{R}\right) m_{\mathrm{cry}}.$$

In consequence,

$$\frac{dm_{\mathrm{H_2O}}}{dt} = -\frac{dm_{\mathrm{H_2O \subset cry}}}{dt} + \dot{m}^{\pm}_{\mathrm{H_2O}} = -\left(1 - \frac{1}{R}\right) \frac{dm_{\mathrm{cry}}}{dt} + \dot{m}^{\pm}_{\mathrm{H_2O}}, \tag{9}$$

where $\dot{m}^{\pm}_{\mathrm{H_2O}}$ includes for instance the feed of water during the semi-batch mode. The interpretation is that the variation of the free water mass $m_{\mathrm{H_2O}}$ is due to the inclusion of water molecules in crystals where it is bound, and to external sources or sinks.

Combining (9) and (5) allows us now to establish the solvent mass balance. Since in our experiment there will only be a source and no sink, i.e., $\dot{m}^{-}_{\mathrm{H_2O}} = 0$, we shall switch to the notation $q_{\mathrm{H_2O}} := \dot{m}^{+}_{\mathrm{H_2O}}$:

$$\frac{dm_{\mathrm{H_2O}}(t)}{dt} = (R^{-1} - 1) 3 k_v \rho_{\mathrm{cry}} G\left(c_\alpha(t), c_\beta(t), T(t)\right) V(t) \mu_2(t) + q_{\mathrm{H_2O}}(t). \tag{10}$$

2.4 Mass balance of α-lactose

The next step is to include the mass balance for α-lactose in the liquid phase. The variation of mass m_α of α-lactose in the liquid phase is related to the variation of crystal mass m_{cry} and the mass m_β of β-lactose via

$$\begin{aligned} \frac{dm_\alpha(t)}{dt} &= -\frac{1}{R}\frac{dm_{\mathrm{cry}}(t)}{dt} - k_1\left(T(t)\right) m_\alpha(t) + k_2\left(T(t)\right) m_\beta(t) + \dot{m}^{\pm}_\alpha(t) \\ &= -\frac{1}{R}\frac{dm_{\mathrm{cry}}(t)}{dt} + m_{\mathrm{H_2O}}(t)\left[-k_1\left(T(t)\right) c_\alpha(t) + k_2\left(T(t)\right) c_\beta(t)\right] + \dot{m}^{\pm}_\alpha(t). \end{aligned} \tag{11}$$

The factor $1/R$ in the first term takes (8) into account, while the second term models loss and gain of α-lactose in the liquid phase due to mutarotation. The third term $\dot{m}_\alpha^\pm$ regroups external sources and sinks. At the same time we have $m_\alpha = c_\alpha m_{\mathrm{H_2O}}$ by the definition of c_α, so that

$$\frac{dm_\alpha}{dt} = m_{\mathrm{H_2O}} \frac{dc_\alpha}{dt} + c_\alpha \frac{dm_{\mathrm{H_2O}}}{dt}.$$

This leads to

$$m_{\mathrm{H_2O}}(t) \frac{dc_\alpha(t)}{dt} + c_\alpha(t) \frac{dm_{\mathrm{H_2O}}(t)}{dt} = -\frac{1}{R} \frac{dm_{\mathrm{cry}}(t)}{dt} + m_{\mathrm{H_2O}}(t) \left[-k_1\left(T(t)\right) c_\alpha(t) + k_2\left(T(t)\right) c_\beta(t)\right] + \dot{m}_\alpha^\pm(t).$$

Substituting (10) gives

$$m_{\mathrm{H_2O}} \frac{dc_\alpha}{dt} - c_\alpha \left(1 - \frac{1}{R}\right) \frac{dm_{\mathrm{cry}}}{dt} = -\frac{1}{R} \frac{dm_{\mathrm{cry}}}{dt} + m_{\mathrm{H_2O}} \left[-k_1 c_\alpha + k_2 c_\beta\right] + \dot{m}_\alpha^\pm - c_\alpha \dot{m}_{\mathrm{H_2O}}^\pm,$$

which can be simplified to

$$m_{\mathrm{H_2O}} \frac{dc_\alpha}{dt} + \left[\frac{1}{R} - c_\alpha \left(1 - \frac{1}{R}\right)\right] \frac{dm_{\mathrm{cry}}}{dt} = m_{\mathrm{H_2O}} \left[-k_1 c_\alpha + k_2 c_\beta\right] + \dot{m}_\alpha^\pm - c_\alpha \dot{m}_{\mathrm{H_2O}}^\pm.$$

We can interpret the source term $\dot{m}_\alpha^\pm$ as

$$\dot{m}_\alpha^\pm = \dot{c}_\alpha^\pm m_{\mathrm{H_2O}}^\pm + c_\alpha^\pm \dot{m}_{\mathrm{H_2O}}^\pm.$$

Then we obtain

$$m_{\mathrm{H_2O}} \frac{dc_\alpha}{dt} + \left[\frac{1}{R} - c_\alpha \left(1 - \frac{1}{R}\right)\right] \frac{dm_{\mathrm{cry}}}{dt} = m_{\mathrm{H_2O}} \left[-k_1 c_\alpha + k_2 c_\beta\right] + \dot{c}_\alpha^\pm m_{\mathrm{H_2O}}^\pm + \left(c_\alpha^\pm - c_\alpha\right) \dot{m}_{\mathrm{H_2O}}^\pm.$$

Dividing by $m_{\mathrm{H_2O}}$ gives the equation

$$(12)\quad \frac{dc_\alpha}{dt} + \frac{1}{m_{\mathrm{H_2O}}} \left[\frac{1}{R} - c_\alpha \left(1 - \frac{1}{R}\right)\right] \frac{dm_{\mathrm{cry}}}{dt} = -k_1 c_\alpha + k_2 c_\beta + \dot{c}_\alpha^\pm \frac{m_{\mathrm{H_2O}}^\pm}{m_{\mathrm{H_2O}}} + \left(c_\alpha^\pm - c_\alpha\right) \frac{\dot{m}_{\mathrm{H_2O}}^\pm}{m_{\mathrm{H_2O}}}.$$

As we shall see, in our study we have $\dot{c}_\alpha^\pm = 0$ and $c_\alpha^- = 0$, so that we are left with a source term $c_\alpha^+ \frac{\dot{m}_{\mathrm{H_2O}}^+}{m_{\mathrm{H_2O}}} = c_\alpha^+ \frac{q_{\mathrm{H_2O}}}{m_{\mathrm{H_2O}}}$. Moreover, c_α^+ will be chosen constant, which means the fraction of α-lactose in the feed does *not* change, even though the feed rate $q_{\mathrm{H_2O}}(t)$ is time-varying and used to control the process.

2.5 Mass balance of β-lactose

Proceeding in analogous fashion for the mass balance of β-lactose, we have

$$(13)\quad \frac{dm_\beta}{dt} = k_1 m_\alpha - k_2 m_\beta + \dot{m}_\beta^\pm,$$

which accounts for mutarotation and feed. Using

$$\frac{dm_\beta}{dt} = m_{\mathrm{H_2O}} \frac{dc_\beta}{dt} + c_\beta \frac{dm_{\mathrm{H_2O}}}{dt}$$

in tandem with (10), we obtain

$$m_{\mathrm{H_2O}}\frac{dc_\beta}{dt} - c_\beta\left(1-\frac{1}{R}\right)\frac{dm_{\mathrm{cry}}}{dt} = m_{\mathrm{H_2O}}\left[k_1c_\alpha - k_2c_\beta\right] + \dot{m}_\beta^{\pm} - c_\beta\dot{m}_{\mathrm{H_2O}}^{\pm}.$$

Again we interpret $\dot{m}_\beta^{\pm}$ as

$$\dot{m}_\beta^{\pm} = \dot{c}_\beta^{\pm}m_{\mathrm{H_2O}}^{\pm} + c_\beta^{\pm}\dot{m}_{\mathrm{H_2O}}^{\pm},$$

then

$$\frac{dc_\beta}{dt} - \frac{c_\beta}{m_{\mathrm{H_2O}}}\left(1-\frac{1}{R}\right)\frac{dm_{\mathrm{cry}}}{dt} = k_1c_\alpha - k_2c_\beta + \dot{c}_\beta^{\pm}\frac{m_{\mathrm{H_2O}}^{\pm}}{m_{\mathrm{H_2O}}} + \left(c_\beta^{\pm}-c_\beta\right)\frac{\dot{m}_{\mathrm{H_2O}}^{\pm}}{m_{\mathrm{H_2O}}}. \tag{14}$$

The crucial point about equations (12) and (14) is that on substituting (5), the state m_{cry} disappears. As we noticed above, our study uses $\dot{c}_\beta^{\pm} = 0$ and $c_\beta^{-}\dot{m}_{\mathrm{H_2O}}^{-} = 0$, so that the source term is $c_\beta^{+}\frac{\dot{m}_{\mathrm{H_2O}}^{+}}{m_{\mathrm{H_2O}}} = c_\beta^{+}\frac{q_{\mathrm{H_2O}}}{m_{\mathrm{H_2O}}}$, with a fixed c_β^{+}.

2.6 Relating volume of slurry to masses

The total volume of slurry $V(t)$ in the crystallizer is a dependent variable, which we now express as a function of the states c_α, c_β, and $m_{\mathrm{H_2O}}$. Observe that we have the relations

$$V_\alpha = m_\alpha\rho_{\mathrm{lac},\alpha}^{-1}, V_\beta = m_\beta\rho_{\mathrm{lac},\beta}^{-1}, V_{\mathrm{cry}} = m_{\mathrm{cry}}\rho_{\mathrm{cry}}^{-1}, V_{\mathrm{H_2O}} = m_{\mathrm{H_2O}}\rho_{\mathrm{H_2O}}^{-1},$$

with the obvious meanings, so that the total volume is

$$V(t) = V_\alpha(t) + V_\beta(t) + V_{\mathrm{H_2O}}(t) + V_{\mathrm{cry}}(t).$$

Substituting the expressions from the previous sections,

$$V_\alpha = c_\alpha m_{\mathrm{H_2O}}\rho_{\mathrm{lac},\alpha}^{-1}, \qquad V_\beta = c_\beta m_{\mathrm{H_2O}}\rho_{\mathrm{lac},\beta}^{-1}, \qquad V_{\mathrm{H_2O}} = m_{\mathrm{H_2O}}\rho_{\mathrm{H_2O}}^{-1},$$

and using

$$V_{\mathrm{cry}}(t) = \left(k_v\rho_{\mathrm{cry}}V(t)\int_0^\infty n(L,t)L^3dL\right)\rho_{\mathrm{cry}}^{-1} = k_vV(t)\int_0^\infty n(L,t)L^3dL,$$

we obtain

$$V(t)\left(1-k_v\int_0^\infty n(L,t)L^3dL\right) = m_{\mathrm{H_2O}}(t)\left[c_\alpha(t)\rho_{\mathrm{lac},\alpha}^{-1} + c_\beta(t)\rho_{\mathrm{lac},\beta}^{-1} + \rho_{\mathrm{H_2O}}^{-1}\right].$$

Using the third moment this may be written as

$$V(t) = \frac{m_{\mathrm{H_2O}}(t)}{1-k_v\mu_3(t)}\left[\rho_{\mathrm{lac},\alpha}^{-1}c_\alpha(t) + \rho_{\mathrm{lac},\beta}^{-1}c_\beta(t) + \rho_{\mathrm{H_2O}}^{-1}\right]. \tag{15}$$

This expression will have to be substituted for $V(t)$ in the formulae below and above. Then the initial condition $V(0) = V_0$ leads to

$$\frac{m_{\mathrm{H_2O}}(0)}{1-k_v\mu_3(0)}\left[\rho_{\mathrm{lac},\alpha}^{-1}c_\alpha(0) + \rho_{\mathrm{lac},\beta}^{-1}c_\beta(0) + \rho_{\mathrm{H_2O}}^{-1}\right] = V_0. \tag{16}$$

Here $\mu_3(0) = \int_0^\infty n_0(L)L^3dL = \frac{m_{\mathrm{cry},0}}{\rho_{\mathrm{cry}}k_vV_0}$ by (24), and $m_{\mathrm{H_2O}}(0) = m_{\mathrm{H_2O},0}$, which when substituted into (16) gives the initial condition

$$V_0 = m_{\mathrm{cry},0}\rho_{\mathrm{cry}}^{-1} + m_{\mathrm{H_2O},0}\left[\rho_{\mathrm{lac},\alpha}^{-1}c_{\alpha,0} + \rho_{\mathrm{lac},\beta}^{-1}c_{\beta,0} + \rho_{\mathrm{H_2O}}^{-1}\right]. \tag{17}$$

In addition, if we assume that α-and β-lactose are initially at an equilibrium of mutarotation, we have to add the initial condition

$$c_{\beta,0} = k_m(T_0)c_{\alpha,0}, \tag{18}$$

where $T(0) = T_0$ is the initial temperature of the slurry. Clearly if $m_{\mathrm{H_2O},0}$ and $c_{\alpha,0}$, $c_{\beta,0}$ are known, we also know V_0. Conversely, if V_0 and $c_{\alpha,0}$, $c_{\beta,0}$ are known, we can determine $m_{\mathrm{H_2O},0}$. Likewise, since we assume that α and β are initially at equilibrium of mutarotation, it suffices to know V_0 and $c_{\alpha,0} + c_{\beta,0}$ to reconstruct $m_{\mathrm{H_2O},0}$. Quantities depending on temperature and initial values given respectively in Table 4 and Table 5.

We also need a formula for $\frac{dV}{dt}$, because it arises in the population balance equation. Differentiation of (15) multiplied by $(1 - k_v\mu_3)$ gives

$$\begin{aligned}&\frac{dV(t)}{dt}\left(1 - k_v\mu_3(t)\right) - V(t)k_v\frac{d\mu_3(t)}{dt}\\ &\quad= \frac{dm_{\mathrm{H_2O}}(t)}{dt}\left[\rho_{\mathrm{lac},\alpha}^{-1}c_\alpha(t) + \rho_{\mathrm{lac},\beta}^{-1}c_\beta(t) + \rho_{\mathrm{H_2O}}^{-1}\right] + m_{\mathrm{H_2O}}(t)\left(\rho_{\mathrm{lac},\alpha}^{-1}\frac{dc_\alpha(t)}{dt} + \rho_{\mathrm{lac},\beta}^{-1}\frac{dc_\beta(t)}{dt}\right).\end{aligned} \tag{19}$$

Substituting (10), (12), (14) removes all derivative terms on the right hand side of (19). It remains to deal with the expression $\mu_3V' + V\mu_3'$. For this we multiply the population balance equation (1) by L^3 and integrate, so using (6) we obtain

$$V'(t)\mu_3(t) + V(t)\mu_3'(t) + G(c_\alpha(t), c_\beta(t), T(t))V(t)\int_0^\infty \frac{\partial n(L,t)}{\partial L}L^3dL = 0,$$

and by partial integration

$$V'(t)\mu_3(t) + V(t)\mu_3'(t) - 3G(c_\alpha(t), c_\beta(t), T(t))V(t)\int_0^\infty n(L,t)L^2dL = 0.$$

Substituting this in (19) gives

$$\begin{aligned}\frac{dV(t)}{dt} &= 3k_vG(c_\alpha(t), c_\beta(t), T(t))V(t)\mu_2(t) +\\ &\quad\frac{dm_{\mathrm{H_2O}}(t)}{dt}\left[\rho_{\mathrm{lac},\alpha}^{-1}c_\alpha(t) + \rho_{\mathrm{lac},\beta}^{-1}c_\beta(t) + \rho_{\mathrm{H_2O}}^{-1}\right] + m_{\mathrm{H_2O}}(t)\left(\rho_{\mathrm{lac},\alpha}^{-1}\frac{dc_\alpha(t)}{dt} + \rho_{\mathrm{lac},\beta}^{-1}\frac{dc_\beta(t)}{dt}\right).\end{aligned} \tag{20}$$

2.7 Energy balance

The energy balance includes the internal heat produced by the crystallization reaction, and the heating and cooling system used to trigger and control the process. Altogether this involves the state $T(t)$, the temperature of the slurry, assumed homogeneous due to stirring, the temperature of the crystallizer jacket $T_{\mathrm{jacket}}(t)$, and the set-point temperature $T_{\mathrm{sp}}(t)$, which is used as control input. We also need T_{feed}, the temperature of the feed, which we assume constant, and a reference

temperature $T_{\text{ref}} = 25\,^{\circ}C$, needed to quantify the heating respectively cooling effect of the feed on the crystallizer temperature T [2]. This leads to the equation

$$\frac{dT(t)}{dt} = P_1(t)\Big[- P_2(t)(T(t) - T_{\text{ref}}) - \Delta H \frac{dm_{\text{cry}}(t)}{dt} + UA(t)\left(T_{\text{jacket}}(t) - T(t)\right) \\ + q_{H_2O}(t)\left(C^p_{H_2O} + C^p_\alpha c_\alpha(0) + C^p_\beta c_\beta(0)\right)\left(T_{\text{feed}} - T_{\text{ref}}\right)\Big] \tag{21}$$

where

$$\frac{dT_{\text{jacket}}(t)}{dt} = -0.0019(T_{\text{jacket}}(t) - T_{\text{sp}}(t)) \tag{22}$$

was obtained through identification of the system. Notice that $T_{\text{sp}}(t)$ is used as a control input to regulate $T_{\text{jacket}}(t)$, and therefore indirectly $T(t)$, via the heat exchange between the jacket and the crystallizer through the contact surface $A(t)$, which is a dependent function of $V(t)$. Here ΔH is the heat of crystallization in kJ/kg, see [29], and the constants $C^p_{H_2O}$, C^p_α, C^p_β are the specific heat capacities of water, α- and β-lactose. We have used the abbreviations

$$P_1(t)^{-1} = m_{H_2O}(t)C^p_{H_2O} + m_\alpha(t)C^p_\alpha + m_\beta(t)C^p_\beta + m_{\text{cry}}(t)C^p_{\text{cry}},$$

$$P_2(t) = \frac{dm_{H_2O}(t)}{dt}C^p_{H_2O} + \frac{dm_\alpha(t)}{dt}C^p_\alpha + \frac{dm_\beta(t)}{dt}C^p_\beta + \frac{dm_{\text{cry}}(t)}{dt}C^p_{H_2O},$$

with $m_\alpha = c_\alpha m_{H_2O}$, $m_\beta = c_\beta m_{H_2O}$ as before.

2.8 Mutarotation and saturation

The mutarotation exchange coefficients k_1, k_2 depend on temperature via the Arrhenius law

$$k_2(T) = k_0 \exp\left(-\frac{E_a}{R_g(T + 273.15)}\right), \quad k_1(T) = k_2(T)k_m(T),$$

where k_0, E_a are constants, R_g is the gas constant, and where according to [17], k_m follows the affine law

$$k_m(T) = 1.64 - 0.0027 \cdot T.$$

The equilibrium of mutarotation therefore occurs at

$$c_{\alpha,\text{sat,eq}}(T) = \frac{10.9109 \cdot \exp(0.02804 \cdot T)}{100(1 + k_m(T))},$$

so that the saturation level for the formation of α-crystals is also temperature dependent and expressed as

$$c_{\alpha,\text{sat}}(c_\beta, T) = c_{\alpha,\text{sat,eq}}(T) - F(T)(c_\beta - k_m(T)c_{\alpha,\text{sat,eq}}(T)),$$

with $F(T) = 0.0187 \cdot \exp(0.0236 \cdot T)$ a correction factor for α-lactose solubility following a Visser type law according to [17]. Note that the saturation concentration varies in time as $c_{\alpha,\text{sat}}(c_\beta(t), T(t))$, because $c_\beta(t)$ and $T(t)$ vary in time.

2.9 Nucleation and growth rates

The nucleation and growth rates are based on phenomenological laws which are usually determined experimentally. Following [17], we used the birth rate

$$B(c_\alpha, c_\beta, T) = k_b \exp\left(-\frac{B_0}{(T+273.15)^3 \ln^2\left(\frac{c_\alpha}{c_{\alpha,\mathrm{sat}}(c_\beta,T)}\right)}\right)$$

for $c_\alpha > c_{\alpha,\mathrm{sat}}$, while $B(c_\alpha, c_\beta, T) = 0$ for $c_\alpha \leq c_{\alpha,\mathrm{sat}}(c_\beta, T)$. Constant k_b given in Table 3 determines the unit of B, while the unit of B_0 is $^\circ C$ [18, 20].

Similarly, the growth rate was based on [17] and chosen as

$$G(c_\alpha, c_\beta, T) = k_g \left(c_\alpha - c_{\alpha,\mathrm{sat}}(c_\beta, T)\right),$$

with unit determined by the unit of the growth coefficient k_g in $m \cdot s^{-1}$. As we can see, $c_\alpha > c_{\alpha,\mathrm{sat}}$ leads to $G > 0$, in which case crystals grow, while $c_\alpha < c_{\alpha,\mathrm{sat}}$ means crystals shrink.

$n(L,t)$	$\sharp/m.m^3$	particle size distribution
$m_\alpha(t)$	kg	mass of α-lactose in solution
$m_\beta(t)$	kg	mass of β-lactose in solution
$V(t)$	m^3	volume of slurry
$A(t)$	m^2	contact surface

TABLE 2: Units of dynamic quantities

3 Modeling for control

In this section we present techniques which allow to control the model presented in the previous chapter. We discuss the moment approach, indicate how it can be extended to include attrition, and then discuss appropriate cost functions.

3.1 Moments

When breakage and agglomeration terms $\dot{n}(L,t)^\pm$ are neglected, one can easily handle the population balance (1) via the moment approach. Putting

$$\mu_i(t) = \int_0^\infty n(L,t) L^i dL, i = 0, 1, \ldots, N,$$

where $N \geq 3$ is the number of moments we wish to consider, we multiply the population balance equation by L^i and integrate to obtain

$$\frac{d\mu_i(t)}{dt} + \frac{V'(t)}{V(t)}\mu_i(t) - iG(c_\alpha(t), c_\beta(t), T(t))\mu_{i-1}(t) = 0, \quad i = 1, 2, \ldots, N, \tag{23}$$

using $\lim_{L\to\infty} L^i n(L,t) = 0$. For the zeroth moment we have the equation

$$\frac{d\mu_0(t)}{dt} + \frac{V'(t)}{V(t)}\mu_0(t) - B(c_\alpha(t), c_\beta(t), T(t)) = 0. \tag{24}$$

The remaining ordinary differential equations (12), (14), (10) in tandem with the energy balance carry over to the moment approach.

Using moments, we write $V(t)$ as a dependent function using (15), while $V'(t)$ uses (20). Altogether, we have a system of ODEs with $N+5$ states $T(t), m_{\mathrm{H_2O}}(t), c_\alpha(t), c_\beta(t)$, in tandem with $\mu_0, \mu_1, \mu_2, \mu_3, \ldots, \mu_N$ with $N \geq 3$. The unknown seed $n_0(L)$ is replaced by its unknown moments $p_i := \int_0^\infty n_0(L) L^i dL$, $i = 0, \ldots, N$. The initial conditions are then

$$\mu_i(0) = p_i, \quad i = 0, \ldots, N, i \neq 3, \tag{25}$$

while the third moment is fixed by fixing the mass of the crystal seed $n_0(L)$.

It is possible to adapt the moment approach to include attrition. Here the source and sink terms are

$$\dot{n}^+_{\mathrm{att}}(L,t) - \dot{n}^-_{\mathrm{att}}(L,t) = \int_L^\infty b(L')\beta(L' \to L) n(L',t) dL' - b(L) n(L,t),$$

where $b(L')$ is the breakage rate of crystals of size L', with unit s^{-1}, and $\beta(L' \to L)$ is the daughter size distribution, with unit m^{-1}. We assume binary breakage, where a particle of volume $k_v L'^3$ breaks into two pieces of volumes $k_v L^3$ and $k_v L''^3$, with $L'^3 = L^3 + L''^3$. We assume symmetry of breakage $\beta(L' \to L) = \beta(L' \to L'')$ and preservation of mass respectively volume

$$\int_0^{L'} \beta(L' \to L) L^3 dL = L'^3. \tag{26}$$

The fact that breakage is binary means

$$\int_0^{L'} \beta(L' \to L) dL = 2, \tag{27}$$

while by symmetry

$$\int_{2^{-1/3}L'}^{L'} \beta(L' \to L) dL = \int_0^{2^{-1/3}L'} \beta(L' \to L'') dL = 1,$$

which shows that $\beta(L' \to L)$ is a probability distribution on the interval $[2^{-1/3}L', L']$. With these assumptions we have indeed

$$\begin{aligned} \int_0^\infty \dot{n}^+_{\mathrm{att}}(L,t) L^3 dL &= \int_0^\infty b(L') n(L',t) \left\{ \int_0^{L'} \beta(L' \to L) L^3 dL \right\} dL' \\ &= \int_0^\infty b(L') n(L',t) L'^3 dL' = \int_0^\infty \dot{n}^-_{\mathrm{att}}(L',t) L'^3 dL', \end{aligned}$$

which is (6) in the case of attrition.

It is standard to assume a self-similar daughter distribution of the form

$$\beta(L' \to L) = \frac{\theta(L^3/L'^3)}{L'},$$

where $\theta : [0,1] \to \mathbb{R}$ is a probability density on $[\frac{1}{2}, 1]$ and symmetric $\theta(1-t) = \theta(t)$. Then with the substitution $L = tL'$ and $dL = L'dt$ we obtain

$$\int_0^{L'} \beta(L' \to L) dL = \int_0^1 \beta(L' \to tL') L' dt = \int_0^1 \frac{\theta(t^3)}{L'} L' dt = \int_0^1 \theta(t^3) dt = 2.$$

If the moment approach is chosen, then we have to evaluate the integrals

$$\begin{aligned}
\int_0^\infty \left(\dot{n}^+_{\text{att}}(L,t) - \dot{n}^-_{\text{att}}(L,t)\right) L^\nu dL &= \int_0^\infty \int_L^\infty b(L') \frac{\theta(L^3/L'^3)}{L'} n(L',t) dL' L^\nu dL - \int_0^\infty b(L) n(L,t) L^\nu dL \\
&= \int_0^\infty \frac{b(L')}{L'} n(L',t) \int_0^{L'} \theta(L^3/L'^3) L^\nu dL dL' - \int_0^\infty b(L) n(L,t) L^\nu dL \\
&= \int_0^\infty \frac{b(L')}{L'} n(L',t) \int_0^1 \theta(t^3) t^\nu L'^\nu L' dt dL' - \int_0^\infty b(L) n(L,t) L^\nu dL \\
&= \int_0^\infty b(L') n(L',t) L'^\nu M_\nu(\theta) dL' - \int_0^\infty b(L) n(L,t) L^\nu dL \\
&= \int_0^\infty (M_\nu(\theta) - 1) L^\nu b(L) n(L,t) dL,
\end{aligned} \tag{28}$$

where $M_\nu(\theta)$ is the ν^{th} moment of $t \mapsto \theta(t^3)$. Since $M_0(\theta) = 2$, we have

$$\int_0^\infty \left(\dot{n}^+_{\text{att}}(L,t) - \dot{n}^-_{\text{att}}(L,t)\right) dL = \int_0^\infty b(L) n(L,t) dL,$$

which is the total number of particles being broken. Moreover

$$L'^3 = \int_0^{L'} \beta(L' \to L) L^3 dL = \int_0^1 \frac{\theta(t^3)}{L'} (tL')^3 L' dt = L'^3 \int_0^1 \theta(t^3) t^3 dt$$

shows $M_3(\theta) = 1$, which confirms again that $\int_0^\infty \left(\dot{n}^+_{\text{att}}(L,t) - \dot{n}^-_{\text{att}}(L,t)\right) L^3 dL = 0$.

Let us now examine how we can compute integrals of the form $\int_0^\infty a(L) n(L,t) dL$ using the moments $\mu_0(t), \ldots, \mu_r(t)$ of $n(\cdot, t)$. Suppose $a(L) \geq 0$ is a weight function in the sense that $\int_0^\infty L^\nu a(L) dL < \infty$ for all ν, and $a(L) \geq 0$. We build orthogonal polynomials with respect to the weight $a(L)$, that is, $\text{span}\{1, \ldots, L^r\} = \text{span}\{P_0, \ldots, P_r\}$ and $\int_0^\infty P_i(L) P_j(L) a(L) dL = \delta_{ij}$ and $P_0 \equiv 1$. If we know an approximation $n(L,t) \approx c_0(t) P_0(L) + \cdots + c_r(t) P_r(L)$, we readily get the approximation

$$\int_0^\infty a(L) n(L,t) dL \approx \sum_{i=0}^r c_i(t) \int_0^\infty P_i(L) a(L) dL = c_0(t).$$

How do we compute the approximation $n(L,t) \approx c_0(t) P_0(L) + \cdots + c_r(t) P_r(L)$? Such an approximation cannot be available on all of $[0, \infty)$, but if $a(L)$ has compact support $[0, L_{\max}]$ say, then it suffices to approximate $n(L,t)$ on this interval. Computing a new orthogonal sequence $Q_0, \ldots, Q_r$ such that $\text{span}\{1, \ldots, L^r\} = \text{span}\{Q_0, \ldots, Q_r\}$ and $\int_0^{L_{\max}} Q_i(L) Q_j(L) dL = \delta_{ij}$, we have

$$n(L,t) \approx d_0(t) Q_0(L) + \cdots + d_r(t) Q_r(L), \tag{29}$$

hence

$$\int_0^{L_{\max}} n(L,t) Q_i(L) dL \approx \sum_{j=0}^r d_j(t) \int_0^{L_{\max}} Q_j(L) Q_i(L) dL = d_i(t).$$

Now every Q_i is of the form $Q_i = \sum_{j=0}^{r} q_{ij} L^j$, hence

$$d_i(t) \approx \sum_{j=0}^{r} q_{ij} \mu_j(t), \tag{30}$$

where we approximate $\int_0^{L_{\max}} n(L,t) L^i dL \approx \mu_i(t)$. Notice that these coefficients q_{ij} are independent of $a(L)$ and depend only on the choice of $L_{\max}$. They may in particular be pre-computed.

From (29) and (30) we obtain the desired approximation of $n(L,t)$ in the bases P_i, i.e., we obtain the coefficients $c_i(t)$, and in particular, $c_0(t)$, as a linear combination of moments. Indeed,

$$Q_i(L) = \sum_{j=0}^{r} e_{ij}(a,t) P_j(L),$$

and then

$$n(L,t) \approx \sum_{i=0}^{r} d_i(t) Q_i(L) = \sum_{j=0}^{r} \left(\sum_{i=0}^{r} e_{ij}(a,t) d_i(t) \right) P_j(L),$$

which gives

$$c_j(t) = \sum_{i=0}^{r} e_{ij}(a,t) d_i(t) = \sum_{k=0}^{r} \left(\sum_{i=0}^{r} e_{ij}(a,t) q_{jk} \right) \mu_k(t).$$

In particular,

$$\int_0^{\infty} a(L) n(L,t) dL \approx \sum_{k=0}^{r} \left(\sum_{i=0}^{r} e_{i0}(a,t) q_{0k} \right) \mu_k(t).$$

In (28) we have to apply this successively to the functions $L \mapsto L^\nu b(L)$, $\nu = 0, \ldots, r$. Notice that $L^\nu b(L)$ is a weight function as soon as b is one.

3.2 The cost function

The criterion we would like to optimize is

$$\max_{u,w,n_0(L),\ldots} k_v \rho_{\text{lac}} V(t_f) \int_{L_1}^{L_2} n(L,t_f) L^3 dL, \tag{31}$$

where t_f is the final time, and where $[L_1, L_2]$ is the interval of sizes in which we want crystals to lie. In our experiments we use $L_1 = 130\,\mu m$, $L_2 = 330\,\mu m$. However, this criterion cannot be used directly in the moment approach.

If we want to continue to use the moment approach, we must either approximate (31) in a way similar to the approximation of the scattering kernel in the previous section, or we may proceed as follows. We choose a target particle size distribution $n_{\text{target}}(L)$, which has its bulk of crystal mass in the range $[L_1, L_2]$, and is then normalized to satisfy

$$\int_0^{\infty} n_{\text{target}}(L) L^3 dL = 1.$$

Now we compute the moments of the target, $\nu_0, \ldots, \nu_N$. Then we replace (31) by the least squares objective

$$\min_{u,w,\mu_i(0),\ldots} \sum_{i=0}^{N} \left(\mu_i(t_f) - \mu_3(t_f)\nu_i\right)^2 . \tag{32}$$

In other words, we bring the moments $\mu_i(t_f)$ of the unknown CSD $n(L,t)$ as close as possible to the moments of the scaled target $\mu_3(t_f)n_{\text{target}}(L)$ by optimizing moments $\mu_i(0)$ and using the controls $u_1 = T_{\text{sp}}$ and $u_2 = q_{\text{H}_2\text{O}}$. This leads us to the following optimal control problem

$$\begin{aligned}
&\text{minimize} && \sum_{i=0}^{N} w_i \left(\mu_i(t_f) - \mu_3(t_f)\nu_i\right)^2 \\
&\text{subject to} && \text{dynamics (23), (24), (10), (12), (14), (21), (22)} \\
&&& \text{initial conditions in table 5} \\
&&& \text{parameters } \mu_i(0) = p_i, i = 0, \ldots, N, i \neq 3 \\
&&& V_0 \leq V(t) \leq V_{\max} \\
&&& 0\,^\circ C \leq T(t) \leq 70\,^\circ C \\
&&& c_\alpha(t) \geq c_{\alpha,\text{sat}}\left(c_\beta(t), T(t)\right)
\end{aligned} \tag{33}$$

with a weighted least-squares objective. The optimization variable is $(T_{\text{sp}}, q_{\text{H}_2\text{O}}, p)$, and the optimal solution is denoted $(T^*_{\text{sp}}, q^*_{\text{H}_2\text{O}}, p^*)$. For the purpose of comparison we have also used a non-specific criterion known in the literature, the mean size diameter $d_{43} = \mu_4(t_f)/\mu_3(t_f)$, which is minimized subject to the constraints of (33).

3.3 Reconstructing the optimal seed

Once the optimal $u_1^* = T^*_{\text{sp}}$, $u_2^* = q^*_{\text{H}_2\text{O}}$, and the optimal moments $\mu_0^*(0) = p_0^*, \ldots, \mu_N^*(0) = p_N^*$ have been computed by (33) or its non-specific variant, we still have to estimate a seed $n_0^*(L)$ which gives rise to these moments. To do this we perform a maximum entropy moment reconstruction, which has the advantage to produce a solution $n_0(L) \geq 0$, see [22, 23]. That is, we seek the function $n_0^*(L)$ which solves

$$\begin{aligned}
&\text{minimize} && \int_0^\infty n_0(L) \ln n_0(L) dL \\
&\text{subject to} && \int_0^\infty n_0(L) L^i dL = p_i^*, i = 0, \ldots, N
\end{aligned} \tag{34}$$

Then $n_0^*(L)$ has its first N moments equal to the μ_i^*, and is in addition positive. If N is small, then the information in $n_0^*(L)$ will not be very significant, but already $N = 4$ gives meaningful results.

4 Experiments

Along with a plethora of heuristics, control of crystallization processes also uses optimal control with non-specific cost functions like the mean size diameter $d_{43} = \frac{\mu_4(t_f)}{\mu_3(t_f)}$ and the nucleation rate B, to enhance product quality. In this study we prefer specific objectives, which allows to maximize the crystal mass produced in a given size range $[L_1, L_2]$. We present results obtained via

program (33), which we compare to one of the non-specific objectives d_{43}. The simulation study is based on experimental conditions for a laboratory size crystallizer. Experimental validation of the novel control strategies obtained in our simulation results is currently under investigation, and experiments were previously used to identify the cooling/heating system of the crystallizer.

4.1 Algorithm

We have used the following overall scheme:

Algorithm 1. Specific maximization of crystal mass

1: **Pose problem.** Select a specific range $[L_1, L_2]$ in which the bulk of crystal mass is desired.
2: **Define target**. Specify target crystal size distribution $n_{\text{target}}(L)$ which fits the chosen interval $[L_1, L_2]$. Normalize to have $\int_0^\infty n_{\text{target}}(L)L^3 dL = 1$.
3: **Optimize.** Select the relevant number of moments N and solve program (33). The solution is $(T^*_{\text{sp}}, q^*_{\text{H}_2\text{O}}, p^*)$.
4: **Maxent reconstruction**. Estimate the optimal seed $n_0(L)^*$ using maximum entropy moment reconstruction (34) from the optimal moments $p^* = (\mu_0^*, \ldots, \mu_N^*)$.
5: **Simulate**. Run the full population dynamic model to validate the results, using $n_0^*(L)$ as seed and $u_1^* = T^*_{\text{sp}}$, $u_2^* = q^*_{\text{H}_2\text{O}}$ as controls.
6: **Evaluate**. If the mismatch between full model and moment model is significant, increase number N of relevant moments and go back to step 3. Otherwise stop.

The target CSD $n_{\text{target}}(L)$ required for the specific optimization program (33) can be chosen in various ways. It is possible to choose a Gaussian distribution centered at $(L_1 + L_2)/2$ such that 90 % of its surface is within $[L_1, L_2]$, and normalized to give a unit integral. In our testing we have used $\sigma = 0.4 \cdot 10^{-4}$. For the specific interval $[L_1, L_2] = [130\,\mu m, 330\,\mu m]$ used in our study we have also used a translated Weibull distribution of the form

$$w(L) = \begin{cases} (5000(L-\theta))^5 \exp\left(-(5000(L-\theta))^5\right), & L \geq \theta \\ 0 & L < \theta \end{cases}$$

where $\theta = 1.371 \cdot 10^{-5}$, normalized to give $n_{\text{target}}(L) = w(L)/\int_0^\infty w(L')L'^3 dL'$ will do.

We have compared the two scenarios by integrating $L^3 n(L, t_f)$ over the target size range $[L_1, L_2]$. The results are shown in Table 6 and corroborate the visual result of Figure 2. Notice that the scaled target and the optimal solution of (33) for the specific criterion have the same crystal mass on $[0, \infty)$ by construction, but a slight difference occurs on $[L_1, L_2]$.

In Figures 3 we present the optimal regulation of set-point temperature and feed rate. For the specific criterion, set-point temperature decreases until $0.2\,h$, keeps an almost constant level for approximately $2\,h$, and then further decreases after $2.5\,h$ with a slight rebound in the end. In contrast the non-specific case shows a mildly increasing set-point temperature during $2.5\,h$, followed by a rapid decrease toward the end.

In the same figure, specific and non-specific optimal feed rate are displayed. For the specific criterion the rate increases steadily from the beginning, whereas the non-specific criterion wants a strong rate for a short period of time, followed by an almost constant rate till the end.

In Figures 4, 5 we present the profile of growth, nucleation rate, solubility and temperature of the crystallizer. Figures 6, 7 present the profile of mass of solvent and mass of solid which

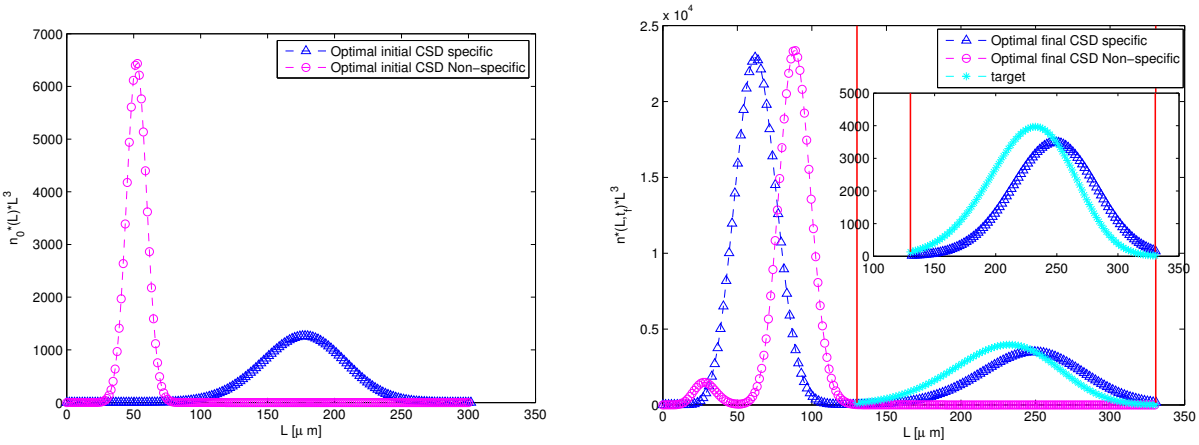

FIGURE 2: Left image shows $n_0^*(L)L^3$ specific (blue) and non-specific (magenta), both estimated via MAXENT from optimal moments $\mu_0^*(0), \ldots, \mu_N^*(0)$. Right image shows the corresponding $n^*(L, t_f)L^3$ for specific (blue) and non-specific (magenta) obtained via (33). The target is shown in cyan. The target range bounds L_1, L_2 are shown in red.

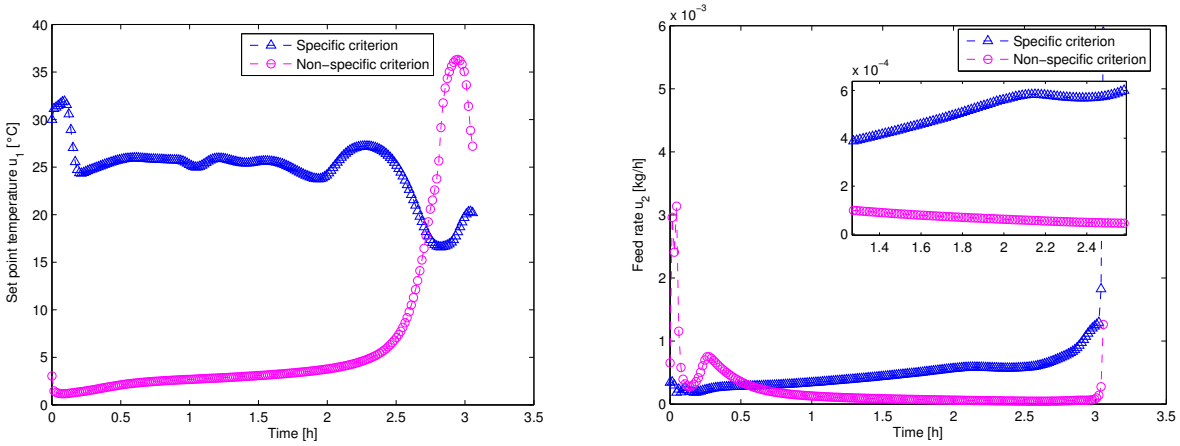

FIGURE 3: Optimal set-point temperature profile $u_1^* = T_{\text{sp}}^*$ (left), and optimal feed profile $u_2^* = q_{\text{H}_2\text{O}}^*$ (right). Specific criterion in blue, non-specific in magenta. Final time t_f was fixed.

are more important in case of specific criterion. The volume profiles show that the crystallizer is entirely filled in the case of the specific criterion, while the crystallizer is not entirely filled for d_{43}. The profile of the weighted mean size diameter over time shows a converging behavior in the end.

4.2 Method

The first step of our testing consists in solving the optimal control problem numerically. Here we have used the solver ACADO [24] based on a semi-direct single or multiple-shooting strategy, including automatic differentiation, and its rationale is the semi-direct multiple-shooting algorithm of Bock and Pitt [25]. ACADO is a self-contained public domain software environment written in `C++` for automatic control and dynamic optimization. Alternatively, we have also used the solver PSOPT [26], which is a public domain extension of the NLP-solver IPOPT [27] or SNOPT [28]

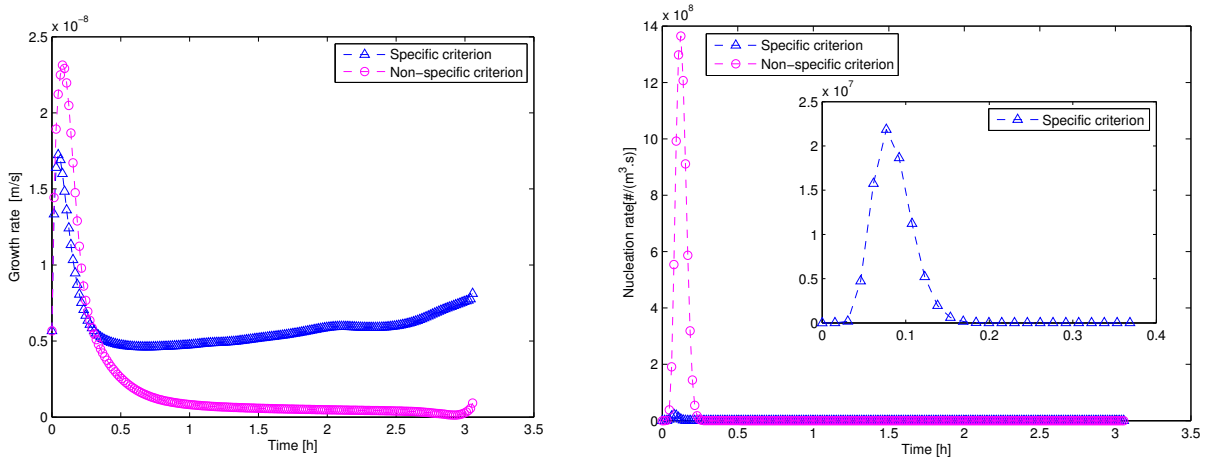

FIGURE 4: Evolution of growth rate G (left) and nucleation rate B (right). Specific (blue) and non-specific criterion (magenta).

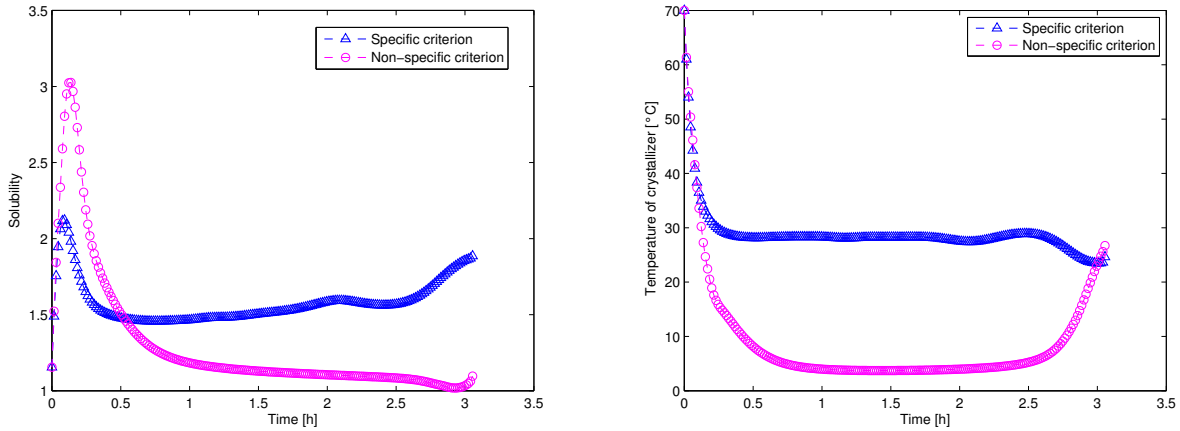

FIGURE 5: Evolution of solubility (left) and temperature of crystallizer (right). Specific criterion (blue), non-specific criterion (magenta).

and is based on pseudospectral optimization which uses Legendre or Cheybyshev polynomials and discretization based on Gauss-Lobatto nodes.

A difficulty with both solvers is the strong dependence of convergence and solutions on the initial guess, as must be expected in a local optimization context. Our testing shows that it is mandatory to have a simulated study $(T^0_{\rm sp}, q^0_{\rm H_2O}, p^0)$ available to start the optimization. This initial guess may use parameters from a previous optimization study, which give already a decent cost in the present study. Homotopy techniques, using for instance t_f as a parameter, have to be used.

In the second step of our testing we use the maximum entropy method to reconstruct the optimal seed $n_0(L)^*$ from its optimal moments $\mu^*_0, \ldots, \mu^*_N$ obtained in the first stage. In the third step of the testing we perform a simulation of the full population dynamic model, using the optimal seed $n^*_0(L)$ in tandem with the optimal controls $u^*_1 = T^*_{\rm sp}$, $u^*_2 = q^*_{\rm H_2O}$ obtained in stage 1. The simulation uses a first-order finite-difference upwind scheme with a backward-space approximation

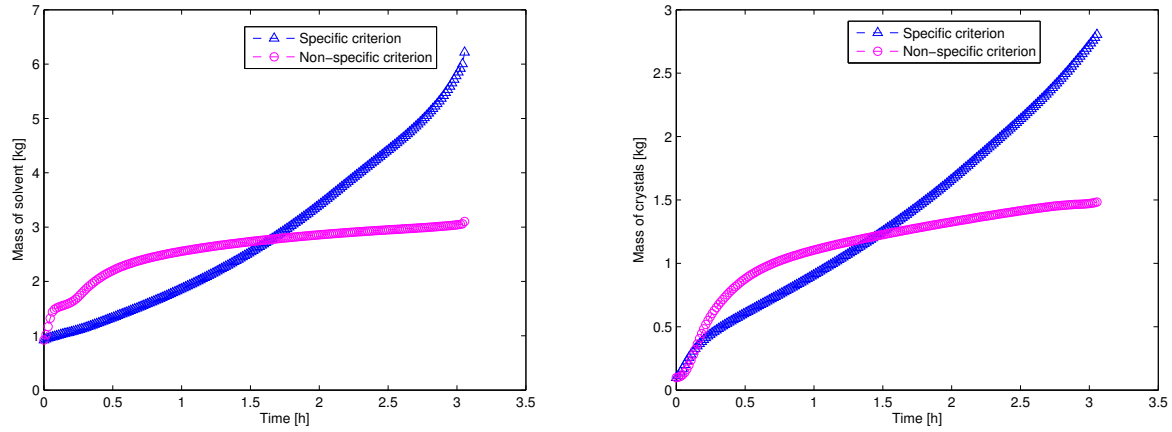

FIGURE 6: Evolution of total mass of solvent $m_{\mathrm{H_20}}$ (left) and of total crystal mass (or solid) m_{cry} (right). Specific criterion (blue), non-specific criterion (magenta).

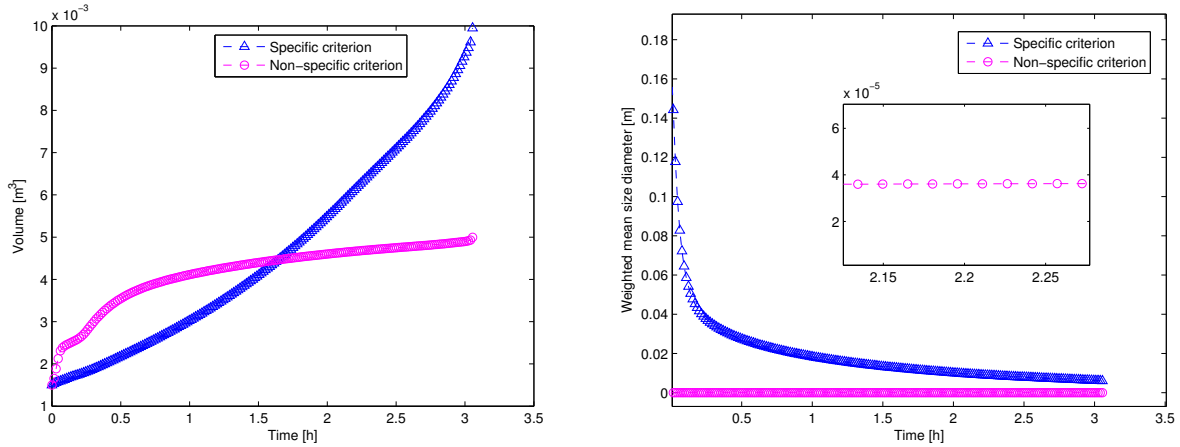

FIGURE 7: Evolution of volume (left) and weighted mean size diameter (right). Specific criterion (blue), non-specific criterion (magenta). Surprisingly, in the nonspecific case the optimal scenario decides to not fill the container entirely.

of $\dfrac{\partial n}{\partial L}$. The last step is to use the full model simulation to reproduce the moment based approach in order to see whether this agrees with the moment method of stage 1.

5 Conclusion

The use of optimal control techniques based on mathematical modeling to enhance product quality in crystallization was discussed. For solvated crystallization of α-lactose monohydrate we were able to show that the crystal mass produced in a specific size range may be substantially increased over standard approaches if optimization is used. Due to the large size of the PDE-based problem, optimization was based on a reduced model for control obtained via the moment approach.

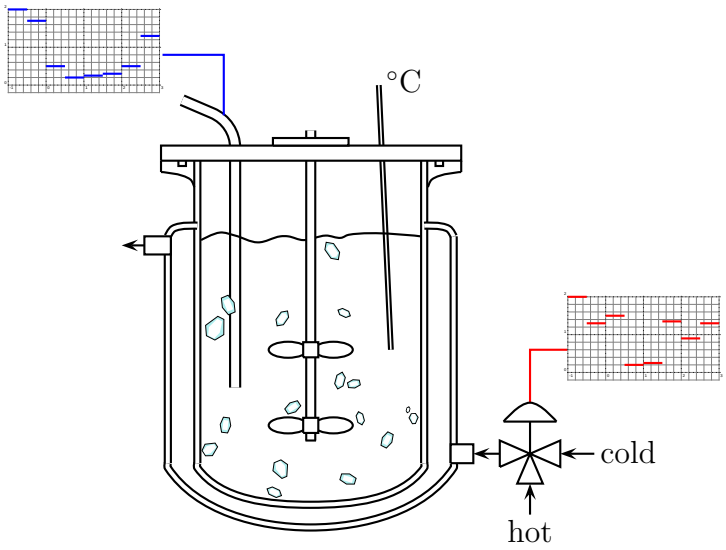

FIGURE 8: 10L crystallizer available at laboratory on which simulations are based.

References

[1] J.W. Mullin, J. Nyvlt. Programmed cooling of batch crystallizers. Chemical Engineering Science, 26, 369377, 1971.

[2] A.Mersmann : Crystallization Technology Handbook, Marcel Dekker, New York, 2001.

[3] A. Randolph, M. A. Larson. Theorie of particulate processes, Academic Press Inc, San Diego, CA, Second Edition., 1988

[4] James B. Rawling, Walter R. Witkowski and John W.Eaton. Modeling and control of crystallizers, Powder technology, volume 6, 1992.

[5] S. Rohani. The dynamic study and control of crystal size distribution (CSD) in Kcl crystallizer. The canadian journal of chemical engineering, volume 64, 1986.

[6] G.P. Zhang and S. Rohani. Online optimal control of a seeded batch cooling crystallizer. Chemical Engineering Science, 58, 18871896, 2003.

[7] Q. Hu, S.Rohani, D.X. Wang, A. Jutan. Optimal control of a batch cooling seeded crystallizer, Powder technology, volume 7, 2005.

[8] J. P. Corriou, S.Rohani. A New Look at Optimal Control of a Batch Crystallizer. American Institute of Chemical Engineers, volume 54, 2008.

[9] M. Sheikhzadeh, M. Trifkovic, S. Rohani. Real-time optimal control of an anti-solvent isothermal semi-batch crystallization process. Chemical Engineering Science, 63 829839, 2008.

[10] A.G. Jones. Optimal operation of a batch cooling crystallizer. Chemical Engineering Science, 29, 10751087, 1974.

[11] J. B. Rawlings, W. R. Witkowski, J. W. Easton. Modelling and control of crystallizers. Powder technology, 69, 39, 1992.

[12] J. A. Thurlby, O. Sitnal. Lactose crystallization: Investigation of some process alternatives. Journal of food science, volume 41, 1976.

[13] J. Bronlund. The modelling of caking in bulk lactose. PhD Thesis, Massey University, 214, 1997.

[14] B. Butler. Modelling industrial of lactose cristallization. PhD Thesis, University of Queensland, 245, 1998.

[15] T. D. Dincer. Mechanisms of lactose cristallization. PhD Thesis, School of applied chemistry, 197, 2000.

[16] Y. Shi, B. Liang, R.W. Hartel. Isothermal crystallization of alpha-lactose monohydrate in a continuous cooling crystallizer, Journal of Food Science, volume 55, 1990.

[17] J. Mcleod. Nucleation and growth of Alpha lactose Monohydrate PhD Thesis, Massey University, volume 220, 2007.

[18] A. Mimouni. Cristallisation du Lactose et apaississement dans les Lactosérums concentrés, PhD Thesis, Ecole Nationale Supérieure Agronomique de Rennes, 2007.

[19] P. L. H. McSweeney, P. F. Fox. Advanced Dairy Chemistry Volume 3: Lactose, Water, Salts and Minor Constituents, Third Edition. University College, Cork, Ireland, 2009.

[20] A. Mimouni, P. Schuck, S. Bouhallab. Isothermal batch crystallisation of alpha-lactose: A kinetic model combining mutarotation, nucleation and growth steps, International Dairy Journal, volume 8, 2009.

[21] G.Gernigon. Modélisation de la cinétique de crystallisation du lactose en solution-modèles-application à la transformation des lactosérums de mozerella, PhD Thesis, 2012.

[22] J.B. Borwein, A. S. Lewis On the convergence of moment problems, American Mathematical Society, Volume 23, Number 1 , May 1991.

[23] J.B. Borwein, A. S. Lewis, M .N. Limber, D. Noll Maximum entropy reconstruction using derivative information part 2: computational results, Numerische Mathematik, Volume 14,May 1995.

[24] D. Ariens, B. Houska, H.J. Ferreau. ACADO Toolkit User's Manual. `http://www.acadotoolkit.org.`, 2010.

[25] H.G. Bock, K.J. Pitt. A multiple shooting algorithm for direct solution of optimal control problems. Proc 9$^{\text{th}}$ IFAC World Congress, Budapest, pp. 243 – 247. Pergamon Press, 1984.

[26] http://www.psopt.org/Home

[27] A. Wächter and L. T. Biegler. On the Implementation of a Primal-Dual Interior Point Filter Line Search Algorithm for Large-Scale Nonlinear Programming. Mathematical Programming, 2006. `https://projects.coin-or.org/Ipopt`.

[28] P. E. Gill, Walter Murray, and M. A. Saunders. SNOPT: An SQP algorithm for Large-Scale Constrained Optimization. SIAM Review, 47(1), 2001. http://www.sbsi-sol-optimize.com/asp/sol product snopt.htm.

[29] Unit operations in food processing
http://www.nzifst.org.nz/unitoperations/conteqseparation10.htm

[30] E. Aamir, Z. K. Nagy, C. D. Rielly, T. Kleinert, B. Judat. Combined Quadrature Method of Moments and Method of Characteristics Approach for Efficient Solution of Population Balance Models for Dynamic Modeling and Crystal Size Distribution Control of Crystalization Processes, Ind. Eng. Chem. Res. 2009, 48, 8575 − 8584.

quantity	symbol	value	unit
maximum volume	$V_{\max}$	0.01	m^3
initial volume	V_0	0.0015	m^3
crystal density	ρ_{cry}	1545	$kg \cdot m^{-3}$
α-lactose density	$\rho_{\text{lac},\alpha}$	1545	$kg \cdot m^{-3}$
β-lactose density	$\rho_{\text{lac},\beta}$	1590	$kg \cdot m^{-3}$
water density	$\rho_{\text{H}_2\text{O}}$	1000	$kg \cdot m^{-3}$
volumic shape factor	k_v	0.523598	–
ratio of molar masses	R	1.0525	–
universal gas constant	R_g	8.314	$J/K/mol$
birth rate coefficient	k_b	10^{10}	$\sharp \cdot m^{-3}s^{-1}$
nucleation constant	B_0	1.4687^8	–
nucleation exponent	b	2	–
growth rate coefficient	k_g	$1.18 \cdot 10^{-7}$	$m \cdot s^{-1}$
growth exponent	g	1	–
activation energy	E_a	$7.4 \cdot 10^4$	J
kinetic mutarotation constant	k_0	$2.25 \cdot 10^8$	s^{-1}
heat of crystallization	ΔH	-43.1	kJ/kg
heat transfer coefficient	U	300	$W/m^2/K$
heat capacity of water	$C^p_{\text{H}_2\text{O}}$	4180.5	$J/kg/K$
heat capacity of α-crystal	C^p_{cry}	1251	$J/kg/K$
heat capacity of α-lactose	C^p_{α}	1193	$J/kg/K$
heat capacity of β-lactose	C^p_{β}	1193	$J/kg/K$
fraction of α-lactose in feed	c^+_{α}	0.521	kg/kg water
fraction of β-lactose in feed	c^+_{β}	0.359	kg/kg water
mass of seed	$m_{\text{cry},0}$	0.1	kg
reference temperature	T_{ref}	25	$°C$
feed temperature	T_{feed}	20	$°C$
final time	t_f	11000	s

TABLE 3: Numerical constants of industrial crystallizer

quantity	symbol	unit
mutarotation exchange fraction	$k_m(T)$	–
mutarotation $\alpha \to \beta$ exchange rate	$k_1(T)$	s^{-1}
mutarotation $\beta \to \alpha$ exchange rate	$k_2(T)$	s^{-1}
saturation concentration at equilibrium of mutarotation	$c_{\alpha,\text{sat,eq}}(T)$	–
saturation concentration	$c_{\alpha,\text{sat}}(c_\beta, T)$	–
crystal growth rate	$G(c_\alpha, c_\beta, T)$	ms^{-1}
crystal birth rate	$B(c_\alpha, c_\beta, T)$	$\sharp \cdot m^{-3}s^{-1}$

TABLE 4: Quantities depending on temperature

m_{cry}	$0.1kg$	$m_{\text{H}_2\text{O}}$	$0.92kg$
V_0	$0.0015m^3$	c_α	0.359
μ_3	0.0812	c_β	0.521
T_{jacket}	20^0C	T	70^0C

TABLE 5: Initial values

Final crystal mass in $[L_1, L_2]$	Expression	Value
Specific criterion	$\rho k_v V(t_f) \int_{L_1}^{L_2} n^*(L, t_f) L^3 dL$	$2.29\,kg$
Scaled target	$\rho k_v V(t_f) \int_{L_1}^{L_2} (\mu_3(t_f)^* n_{\text{target}}(L)) L^3 dL$	$2.80\,kg$
Non-specific criterion	$\rho k_v V(t_f) \int_{L_1}^{L_2} n^*(L, t_f) L^3 dL$	$0.0\,kg$

TABLE 6: Final crystal mass in $[L_1, L_2]$ of case of specific criterion, scaled target and non-specific criterion